A dose delivery verification method for conventional and intensity-modulated radiation therapy using measured field fluence distributions

Wendel Dean Renner[a)]
Math Resolutions, LLC, 5975 Gales Lane, Columbia, Maryland 21045

Mehrdad Sarfaraz, Matthew A. Earl, and Cedric X. Yu
Radiation Oncology Department, University of Maryland Medical Systems, 22 South Greene Street, Baltimore, Maryland 21201

(Received 13 March 2003; revised 29 July 2003; accepted for publication 29 July 2003; published 23 October 2003)

Treatment verification has been a weak link in external beam radiation therapy. As new and more complicated treatment techniques, such as intensity-modulated radiation therapy (IMRT), are implemented into clinical practice, verifying the accuracy of treatment delivery becomes increasingly important. Existing methods for treatment verification are highly labor intensive. We have developed a method for verifying the delivery of external beam radiotherapy and implemented the methodology into a system consisting of both hardware and software components. The system uses grayscale images acquired on the treatment machine from the planned treatment beams. From these images, the photon fluence distribution of each beam is derived. These measured photon fluence maps are then used as input to a separate dose calculation engine to compute the delivered absolute dose and the dose distribution in the same patient, assuming that the patient is set up as required by the treatment plan. The dose distribution generated from the measured fluence maps can then be compared to that of the treatment plan. Software tools, such as overlaying isodose curves generated with this method on those imported from the plan, dose difference maps, dose difference volume histograms, and three-dimensional perspective views of the dose differences, have also been developed. The system thus provides a means to verify the dose, the dose prescription, and the monitor units applied. The potential exists with a suitable electronic portal imaging system to reduce the quality assurance efforts, especially for IMRT. © *2003 American Association of Physicists in Medicine.* [DOI: 10.1118/1.1610771]

Key words: treatment verification, quality assurance, dosimetric verification

I. INTRODUCTION

Delivering the correct dose to the patient as required by the treatment plan requires the satisfaction of two conditions. First, the patient must be set up to reproduce the geometry assumed by the planning system with the correct gantry, couch, and collimator settings. Second, the machine must deliver the correct amount of radiation with the correct field shape settings and the correct energy. The verification of these conditions is generally regarded as treatment verification, which is an area of strong interest in radiation therapy. Even with proper patient positioning, organ motion may be a significant factor in treatment accuracy. Electronic portal imaging systems with and without implanted radio-opaque markers are used clinically at many institutions to verify the geometric accuracy of treatment. Electronic portal imaging has been reported for verifying intensity-modulated radiation therapy (IMRT) dose.[1] Dosimetric measurements to verify the accuracy of beam delivery are also widely practiced clinically. Methods for *in vivo* dosimetry, which attempts to verify all conditions, have also been proposed.[2,3]

In the conventional treatment plans, beams are simple shaped-fields with uniform beam intensities. As long as there is a rigorous quality assurance (QA) program in place to ensure the geometric and machine output accuracy, high accuracy of beam delivery by the machines can be achieved. Practice standards for quality control in radiotherapy have been established over the years and are in the literature.[4,5] A conventional approach for quality control in external beam radiotherapy is to perform frequent machine QAs and carefully review each plan.

As radiation therapy becomes more complicated with the introduction of IMRT including compensating filters and dynamic wedges, the possibilities for delivery error become higher. Thus although human error probably remains one of the most significant potential cause of treatment errors, there is also ample opportunity for machine delivery errors.

With IMRT delivery using multileaf collimators (MLCs), effects of leakage, tongue-and-groove design, and machine variations may not be modeled accurately by the planning system and may cause significant dosimetric differences. The delivery of a small number of monitor units (MUs) may lack the required accuracy in both the beam profile and the output.[6,7] In addition, the delays in the machine control may cause inaccuracies in the segmental dose or even skipping some segments.[8] When a large number of segments is used for IMRT delivery, small geometric errors in the segment shapes can also translate into large dosimetric error.[9] It is for these reasons that it is necessary to verify the beam delivery before a patient is treated with IMRT.

Different approaches for IMRT verification are currently

used by different institutions. One method is to use films and/or electronic portal imaging devices to measure the intensity patterns of the beams.[10] The difficulties of these methods are often in the comparisons with the ideal intensity patterns. Moreover, if a difference is found in the intensity patterns, the impact on the dose distribution inside the patient is not known. Therefore comparing the intensity maps alone may not be sufficient to determine if the planned delivery is acceptable. The ideal feedback loop would be to irradiate an exact model of the patient with report of the measured dose throughout the model. However, this would be impractical to perform on a patient-by-patient basis.

Another approach for IMRT verification currently used by most institutions, including ours, is to substitute the patient with a phantom and calculate the dose distribution on the phantom using the same planning parameters as for the patient.[11–13] The treatment plan is then delivered to the phantom and the resulting measurement is compared with the predicted absolute dose and relative dose distributions. If the measured doses agree with calculated doses in the phantom, one assumes that the beam delivery is accurate. Although practical and valid, this approach has some drawbacks. The point dose measurement for IMRT delivery has significant uncertainties due to the dose gradients in an intensity modulated beam. The measured dose can be sensitive to the chamber size, and the location of the chamber. For example, if the chamber is placed at the gap of two adjacent leaves, the leakage and tongue and groove effect may significantly alter the result. Even with an easy system for measurement,[13] the dose comparison is somewhat abstract in that it is performed on an idealized phantom that has no direct bearing on the patient's anatomy. Using an anthropomorphic phantom improves on the anatomic relevance, some customized modifications of the phantom are needed to allow such measurements inside the phantom.[14] Moreover, to obtain both the absolute dose with a chamber and the relative dose distribution with films may often require delivering the treatment to the phantom twice, making the procedure very effort-intensive. Lastly, if differences do arise, it will be difficult to judge if the dose delivery is acceptable as the resulting dose distribution to the patient is not demonstrated.

This paper describes a method that will reconstruct the dose and dose distribution that the patient receives by measuring the amount of radiation dose delivered for each field, but assuming that the correct energy was selected, and assuming that the accelerator's monitor unit system has been correctly calibrated. The method reports both the absolute dose and the dose distribution which can then be compared to that intended. This check is strictly a dosemetric delivery check, patient positioning or organ motion is not addressed here. But we offer this method as a procedure that can serve to greatly increase confidence that some mistake or malfunction has not been overlooked.

The quality control system introduced here uses the measured photon fluence distributions of each individual treatment field as an input to compute the absolute dose and the dose distribution on the same set of CT images of the patient as used by the treatment plan. The images used for the measurements are calibrated to the treatment machine's reference dose. The setup is used for the QA measurements so that the grayscale of the images can be related to the machine output at the calibration condition and the reconstructed doses can be directly compared to the absolute dose and dose distributions calculated by the treatment planning system. The system thus provides a verification loop from planning to delivery back to the plan. The fact that the dose calculation of the new QA system is independent of that of the planning system also adds redundancy which provides further quality assurance.

The method described here, by reconstructing the dose from the measured field intensities and distribution, will signal the presence of a large error if a large dose difference is obtained, and thus will not depend upon the diligence of an individual discovering an error from the inspection of a treatment plan. It is this point that makes this method valuable for conventional radiation therapy as well.

This approach is simpler than attempting to reconstruct the dose from an exit dose measurement.[3] Rather than use the exit dose to estimate the entrance dose, here the entrance dose is measured directly. This eliminates any uncertainties introduced from deriving the entrance dose from the exit. Further, the checking of the dose prescription and delivery system is separated from the question of correct patient positioning, which may be an advantage.

The potential exists with a suitable electronic portal imaging system that can accurately integrate the dose to significantly reduce quality assurance efforts, especially for IMRT. This would be achieved by using a direct interface from the imaging system to the computer using the quality control method described here.

II. METHODS AND MATERIALS

The general idea of this new treatment delivery verification method is to derive the photon fluence distributions from measured beam profiles for all the planned beams and use them to calculate the dose distribution in the patient. Such beam profiles can be acquired with film, an electronic portal imaging system, or other means. We used film in this study to prove the concept and to test the system.

The beam profile measured with a film at a depth is a function of the dose delivered at that depth from the specific beam. The key to make this method sufficiently accurate is to: (1) establish an accurate MU calibration at a well-controlled calibration condition with the gray levels of the image captured with film; (2) accurately derive the photon fluence distributions from the measured grayscale images; and (3) calculate dose in the patient using the photon fluence maps with acceptable precision. These three key areas will be described separately in the following sections.

A. Film calibration

The main sources of uncertainties in film dosimetry are the inconsistencies of exposure conditions between the calibration condition and measurement condition including variation in film response to different energy spectra, and

second, variations among films and in film processing. These sources of uncertainty need to be reduced to achieve the accuracy that is needed here.

To minimize the first source of uncertainties, we require that the same geometric setup including the depth of measurement, the build-up material, and the distance to the source be used for both the calibration and for QA measurement. Two types of films are available for use in this application. For large number of monitor units (MUs) (>200 MU), Kodak's EDR2 film in Ready Pack is available,[15] while for smaller number of monitor units, Kodak XV-film may be used. In this study films were placed at 100 cm from the source on top of 7.6 cm of Styrofoam™, and covered with material (see the following) to shield from contamination electrons, and exposed to a 10×10 cm^2 uniform radiation field. Calibrated relationships (H–D curves) between the optical density and the delivered dose at the central axis in the calibration condition were established for both films and for two different energies on a SL-20 linear accelerator manufactured by Elekta (Atlanta, GA). The upper limits of the MUs used for the calibrations were set to expose the film to an optical density of approximately 3.0, so that the whole usable ranges of the films were covered. Both 12 and 16 bit film scanners [Vidar (Herndon, VA)] were used for scanning the films and the images were transferred to our verification system for analysis.

To minimize the second source of uncertainties, a new calibration sample was required for each QA measurement. Recalibrating the entire H–D curve for each QA measurement would significantly increase the time and effort for each case. There are several ways to make this step easier. One method is to generate only one calibration exposure each time a case is done and rescale the previously measured H–D curve to agree at this one point. Since changes in film batches and processing chemistry will not cause large changes in the H–D curve, this method should provide reasonable accuracy. To test the validity of this method, we made multiple H–D curve measurements with different lots of V films and in different weeks. We then scaled the first H–D curve with one point taken from later H–D curves and compared the resulting H–D curve with the later curve. As shown in Sec. III, the rescaling achieved better than 1% agreement consistently among multiple weeks and lots of films. The term "rescaling" is referred to as a simple mathematical operation of the H–D curve, by which the values of every point on the curve is multiplied by the ratio of the newly measured optical density for a given dose to that of the original optical density value at the same dose. We would expect this result to hold for other film types, such as the EDR2 film, with similar chemistry and H–D curves that might be employed.

Another method would be to calibrate a step wedge and use a single exposure of the step wedge to generate a new H–D curve for each case. A similar approach has been reported using the MLC.[16]

It should be noted that a sensitometer typically used in radiology is not suitable here for correction for film processing. Besides the much longer exposure times required here, the typical stated stability of these devices is ±0.02 log exposure. This computes to a variation in exposure of $\pm4.7\%$. For our purposes we need greater confidence and would like the exposures to be measured within at least $\pm3\%$.

By minimizing the effects of uncertainties commonly associated with film dosimetry as described earlier, the grayscales of the film measurement can be directly related to the dose at the central axis in the calibration condition, which is in turn related to the output of the machine. For the QA of IMRT delivery, each pixel of the dose image captured with film can be converted (and normalized) to the central axis dose of the calibration condition. These dose images are converted to in-air intensity maps expressed in MUs of the calibration condition, with which the dose in the patient can be calculated using a pencil beam dose calculation algorithm. It is important to note that the MUs converted using this procedure serve as a common measurement unit of the photon fluence or intensities which we will refer to here as relative monitor units (RMU). The RMU is used here as a unit to take into account the field size and accessories that have been inserted into the beam. As an example, if a wedge is in a 20×20 cm field with a wedge factor of 0.5 on the central axis and a scatter collimator factor of 1.04, applying 100 MU will result in a measurement of 52.0 RMU on the central axis.

B. Derivation of photon fluence distribution from film measurements

Note that the use of film here is simpler than using film to measure the dose at depth in an extended phantom[15,17] in that here the film is perpendicular to the central axis of the radiation field and only enough material is used over the film to shield from contamination electrons. Changes in spectrum with depth in a phantom due to scatter is not an issue since the film is not in a phantom. Radial changes in the energy spectrum resulting from beam modifying devices, such as a wedge, have been shown to have a relatively small effect (see Fig. 3).

Since any measurement of the photon fluence will require buildup, and also a shield for contamination electrons, any measurement will distort the measured results. Therefore as the means to judge whether a method for measuring or deriving the fluence is effective, the derived fluence map was used as input to calculate the dose on a profile at depth in a water phantom and that computed profile then compared to the dose profile measured at the same depth.

A 3-mm-thick copper plate was used here for shielding contamination electrons and buildup due to a report[3] that 3 mm of copper resulted in an accurately measured fluence map. We tested 2×2, 5×5, 10×10, and 25×25 cm field sizes using 3.18 mm copper as a shield for therapy verification film, comparing the profiles at depths of 3.4, 5, 10, 20, and 30 cm for 18 MV x rays. The film was placed on top of 7.6 cm of Styrofoam on the treatment couch to minimize the backscatter to the film. The film was at 100 cm from the source and covered with the copper sheet. The calibrated images from the film were used to compute the dose profiles

at depth. The same profiles were measured with a Scanditronix-Wellhofer (Scanditronix-Wellhofer North America, Memphis, TN) beam data acquisition system at the same time. For the 2×2 cm field an ion chamber with 3 mm outer diameter was used. For the other fields a chamber with 5 mm outer diameter was used.

A stringent test of the quality control system is to compute the dose for a 60° wedged field from a film measurement of the field. We tested a 20×20 cm field for both 6 and 18 MV.

C. Dose calculation algorithm and validation

The dose calculation algorithm used in this work was based on a pencil beam superposition algorithm. The dose calculation method used here is similar to pencil beam-based dose calculation methods used clinically in many treatment planning systems today. Pencil beams were generated from Monte Carlo generated point spread functions.[18] These were used with measured percent depth dose to fit a spectrum and generate a composite poly-energetic pencil beam. A radiation field is divided into an array of such pencil beams, and the dose to any point is the sum of the contribution from each pencil beam. Although a pencil beam algorithm is less stringent as compared with superposition methods based on point (voxel) dose-spread-arrays,[19,20] the accuracy of these types of pencil beam methods are well known.[21,22] The dose algorithm of the verification system was validated following well-established code of practice.[5,23,24]

For dose calculation in the patient, the pencil beam kernel is first stretched or compressed according to the radiological depth along the central ray of each pencil beam to obtain the dose distributions of each pencil beam in the patient. This achieves a first-order approximation to account for the effects of inhomogeneities in the patient. These location-specific pencil beam dose distributions are then weighted by the intensity values derived at each pencil beam location from the measured fluence map and superpositioned to get the dose distribution of the broad beam. The algorithm here does not model the accelerator head and accessories since those effects are already included in the measured fluence map.

The penumbra is determined by the spread of the pencil beam and the intensity value from the fluence map used to weight each pencil beam. Because the fluence is measured at a fixed distance from the source, changes in penumbra that might be depth dependent are not accounted for here. For example, the source may be modeled as a primary source and a secondary extended source at the position of the flattening filter.[25] As the secondary source is eclipsed differently then the primary source at different depths, there is a slight change in penumbra. However, this effect is expected to be small and has been ignored in this work.

Beam hardening effects are not explicitly considered in the dose calculation since the weighting of each pencil beam does not consider changes in spectral components. This might limit the accuracy for cases where the beam traverses thick bony anatomy or metal objects. However, many treatment planning systems use a similar approximation with accuracy suitable for clinical purposes. Further corrections are not applied since the fluence map is derived from an image that does not contain spectral information.

To convert the calculated dose to the absolute dose, it is necessary to apply a calibration factor derived from the calibration condition that is used for the particular accelerator, i.e., the field size and depth for which the calibration of the accelerator is specified (typically a $10\times10\ \mathrm{cm}^2$ field size at $d_{\max}$ at either 100 cm source-to-surface distance or 100 cm source-to-detector distance, but could be specified at a deeper depth). This calibration factor is simply the quotient of the stated dose to the computed value for 1 MU, i.e.,

$$C_{\mathrm{cal}} = \text{stated cGy/computed dose at calibration condition.} \quad (1)$$

The denominator in Eq. (1) is computed by summing all the pencil beams over the area of the calibration field with each of the pencil beams scaled by a measured in air profile normalized to 1 MU on the central axis, as is typically done in treatment planning system algorithms. The derived constant is subsequently used to multiply all computed doses to arrive at doses in cGy. The units of the pencil beam kernel may therefore be arbitrary. This calibration factor is generated automatically as part of the software function for generating necessary parameters for dose calculation from measured beam data.

D. Software program

A software program, DOSIMETRY CHECK (Math Resolutions, Columbia, MD) was developed to accomplish the goals of the delivery verification system. In this software field images must first be reduced to one of the following formats: DICOM, TIFF, PNG, or a proprietary (Radiological Imaging Technology, Colorado Springs, CO) format. Film measurements were scanned using both 12 and 16 bit scanners and we did not observe any significant accuracy difference between these two methods.

Multiple H and D curves can be entered and selected for the conversion of the scanned measurement to RMU. As discussed earlier, the H–D curve can be rescaled to force agreement at the calibration point obtained at the same time of the "dry-run" beam delivery, or a new curve entered using a calibrated step wedge. Polynomials are fitted to the H and D curves. The order of fit is adjusted to give the best fit with the data.

With the 12 bit scanner, the resultant dose image was written as a true color TIFF file with five bits assigned the blue field, five to green, and two to red. A special routine was written in our verification software to reconstruct the 12 bit grayscale from this encoded true color TIFF format. The digitized images were transferred to the computer running the delivery verification software from the computer connected to the film scanner.

For each of the beam profile images captured on film, the user must locate the central axis and beam's eye view coordinate system. This is accomplished by projecting the coordinate system on top of the field image and subsequently

moving and rotating the coordinate system to match with the beam fluence image. This may require fiducial marks on the films as described in the following.

The treatment plan may be transferred from the treatment planning system into our program in RTOG or DICOM RT format. The program can import the CT scans and geometry information, such as the isocenter position, the couch, gantry, and collimator angles for each beam. In addition, the three-dimensional (3D) dose matrix from the planning system can also be imported for the purpose of comparison. Each beam must then be associated with the corresponding dose image measured with film.

An important consideration is to preserve the geometry of the field, particularly in reference to the collimator angle. As described earlier, the program uses the convention that the field image is oriented relative to the beam's eye view coordinate axes. These axes rotate with the collimator and therefore the field is measured relative to the unrotated collimator. In addition, the field is viewed from the source side. This requires a method for locking the field image position relative to the central axis and beam's eye view axes. For example, when using Ready Pack film, pinpricks can be used on the axes outside of the field. Since any variation in film density will be interpreted as a change in the field fluence, such marks should be placed outside of the area of the field with some margin where they will not perturb the resultant computed dose distribution. An adequate margin around the field is also needed so that the penumbra outside the beam is properly accounted for.

After each treatment beam is associated with the corresponding measured field, the dose distribution is computed. The isodose curves in units of cGy are displayed and compared to the plan calculated by the treatment planning system. A dose difference volume histogram can be generated and printed if the 3D dose matrix was downloaded from the planning system. The dose or dose difference can be viewed in any reformatted image plane or 3D perspective room view. The displays are similar to those of present treatment planning systems. Outlined regions of interest are also supported for point of reference and may be also downloaded in RTOG format. The body outline must be supplied or regenerated, and the conversion of CT number to density must be specified.

III. RESULTS AND DISCUSSION

A. Verification of consistency in film dosimetry

Figure 1 shows the typical variations in H and D curve observed in the study and the validation of the rescaling with one point. Figure 1(a) shows two H and D curves obtained with films from different batches within the same week and two H and D curves obtained in two different weeks. Figure 1(b) shows the same comparison as Fig. 1(a) after rescaling the original H and D curve with one film calibration point at 60 cGy on the other H and D curve. Without rescaling, the relative difference in optical density among H and D curves can be as high as 5% at higher doses. Due to the shallower slope at high dose values, the related dose error can be up to 10%. After rescaling, all H and D curves can be brought to an agreement of better than 2% in optical density. To reduce the error introduced in the rescaling, one should deliver a dose at 25 cGy or higher but below the film saturation dose. There are subtle differences between V film and EDR2 film that have been reported[15,16,26] which may need to be taken into consideration in implementing this quality control method with film.

B. Verification of the dose calculation algorithm

The pencil beam algorithm was initially tested by using the field fluence from a measured in air profile and comparing the computed and measured isodose curves in a water phantom. The algorithm was further tested by comparing the dose at 297 points measured in a Rando phantom for a large 30×35 cm^2 4 MV field covering the chest and lower head[27] to that computed with our algorithm. For 100 cGy to d_{max} on the central axis the deviation between the measured and the computed dose was 2.86 cGy (2.86% relative to the dose at d_{max}). Another test was done using the protocol defined by Task Group 23 in AAPM Report Number 55.[24] The algorithm was used to compute the dose to points measured in the report. The results are summarized in Table I and show a standard deviation of 0.9% at 4 MV and 1.4% at 18 MV (relative to a dose of 1.0 cGy at d_{max}). These results demonstrate that the pencil beam algorithm was adequately validated.

C. Dose computed from measurement of beam fluence

Shown in Fig. 2 are 18 MV profiles for open fields of 2×2, 5×5, 10×10, and 25×25 cm at depths of 3.4, 5, 10, 20, and 30 cm. These profiles were generated using as the input fluence film measurements filtered by 3.18 mm of copper. Each set of profiles, computed and measured, in Fig. 2 were normalized to the same dose at d_{max} (3.4 cm) on the central axis. The results show that 3.18 mm of copper to shield contamination electrons for 18 MV x rays was an effective technique for exposing the beam films as the dose distribution at depth can be computed with no further corrective processing of the derived fluence map and a significant field size dependency effect was not observed.

The absolute dose agreement will be strictly determined by the accuracy of the film measurement and film calibration curve. For absolute dose, the 10×10 cm film was used to rescale the film calibration curve to agree with 60 MU used to expose the fields. The absolute doses for the 25×25 cm field size were 61.5 cGy vs 60.2 from measured data, for 10×10 cm 56.0 cGy vs 56.1, for 5×5 52.0 vs 52.3. For 2×2 cm field size the method produced a dose of 45.4 cGy. A reliable measured value to compare this to was not available.

Table II shows a detailed quantitative analysis of the profiles presented in Fig. 2 for the data pooled at all depths, normalized as described earlier. The standard deviation of measured versus computed values is reported.

The data in Table II are found to be within the suggested acceptability criteria of AAPM Task Group No. 53:[5] 1.5% in

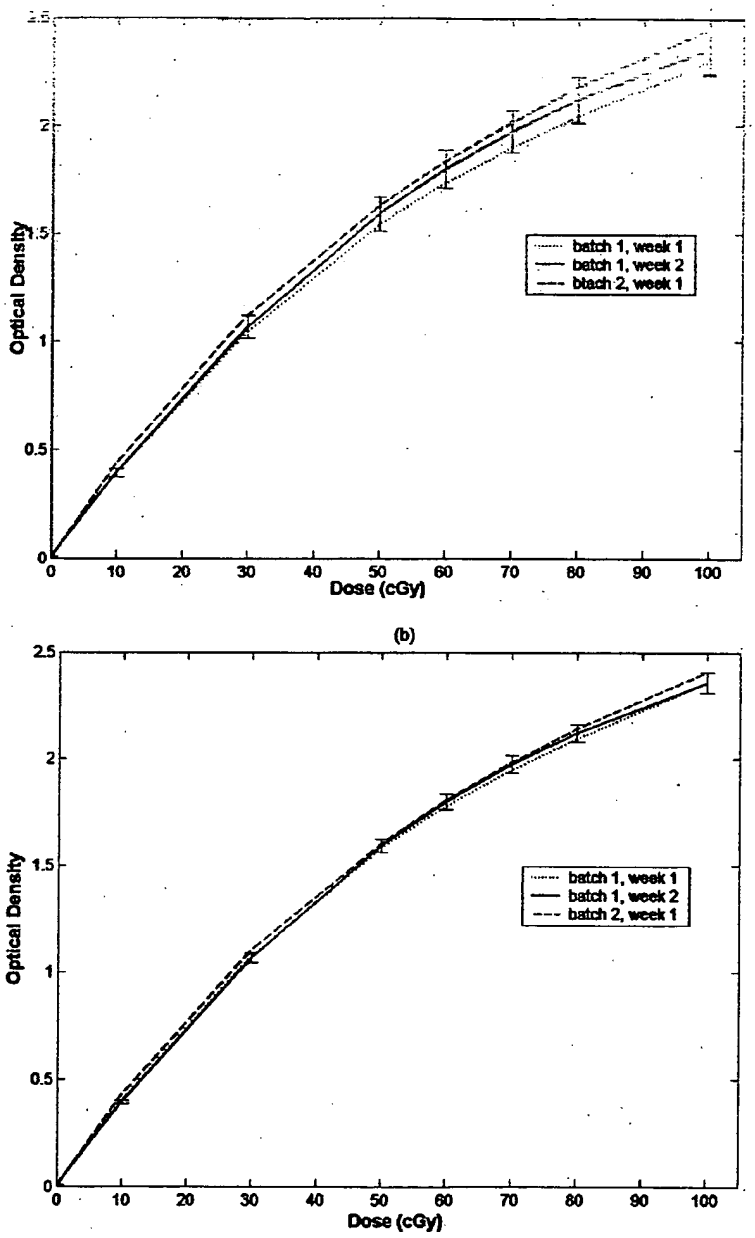

FIG. 1. (a) For films from the same batch in different weeks and films from different batch in same week (error bars represent ±5%). (b) Same films after scaling the films to optical density at 60 cGy (error bars represent ±2%).

the inner beam, 2% in the outer beam, and 2 mm distance-to-agreement in the penumbra region. Shown in Fig. 3 are the 60° wedge, 20×20 cm wedged field profiles for 6 MV [Fig. 3(a)], wedge factor of 0.287, and 18 MV [Fig. 3(b)], wedge factor of 0.298. The curves were normalized to the d_{max} point on the central axis as was done earlier for the open fields in Fig. 2. Table II also includes quantitative data for the wedge profiles. Agreement with measurement for the absolute dose was found to be within 0.5% for 6 MV and 2.0% for 18 MV. These values are within the AAPM TG53 criteria for wedged beams.

TABLE I. Pooled dose difference data from using AAPM Report 55 Radiation Treatment Planning Dosimetry Verification relative to 1 cGy/MU.

Energy (MeV)	Number of points	Standard deviation of dose difference	Average difference in dose	Maximum difference in dose
4	239	0.009	0.000	0.039
18	267	0.014	0.000	0.063

These results are highly dependent upon the film calibration curve. For example, depending upon the order of the polynomial fitted to the film calibration points, the computed profiles at the tip of the wedge in Fig. 3 can be much different than shown here. Care must therefore be taken to use

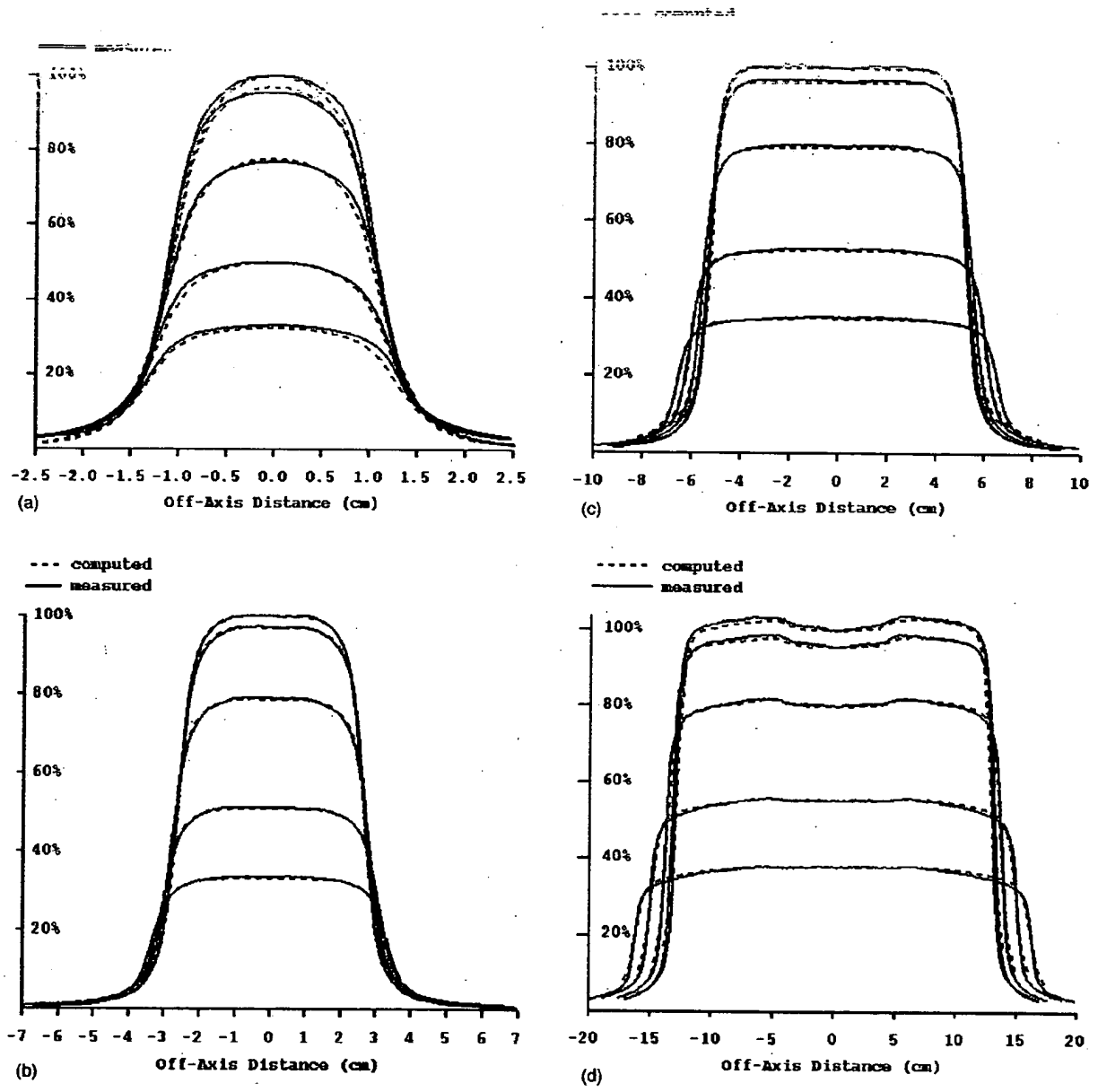

FIG. 2. (a) Computed and measured profiles for a 2×2 cm field. The computed dose is from using 3 mm copper to shield verification film. Depths are 3.4, 5, 10, 20, and 30 cm. Dose normalized to 100% on the central axis at d_{max}. (b) Computed and measured profiles for a 5×5 cm field. The computed dose is from using 3 mm copper to shield verification film. Depths are 3.4, 5, 10, 20, and 30 cm. Dose normalized to 100% on the central axis at d_{max}. (c) Computed and measured profiles for a 10×10 cm field. The computed dose is from using 3 mm copper to shield verification film. Depths are 3.4, 5, 10, 20, and 30 cm. Dose normalized to 100% on the central axis at d_{max}. (d) Computed and measured profiles for a 25×25 cm field. The computed dose is from using 3 mm copper to shield verification film. Depths are 3.4, 5, 10, 20, and 30 cm. Dose normalized to 100% on the central axis at d_{max}.

closely spaced points in the film calibration curve for best results. Replacing film with more accurate technology for measuring the beam fluence would be expected to give better system performance. But accuracy sufficient for verifying a treatment can be obtained with film dosimetry as shown here if measurements are carefully performed.

D. Example of a conf rmal case

Figure 4 shows the transverse slice for a six field conformal prostate case treated at 18 MV x rays. Kodak XV film was used to measure each beam. A 50 MU 10×10 cm test film resulted in 46.6 MU. The calibration curve was then rescaled to produce 50 MU for the test film. The rescaled curve was used to process the beam films. The planning system reported the dose to isocenter to be 203.4 cGy, compared to the value of 201.4 cGy computed here (a 1.0% difference). The hot spot in the treatment volume reported by the planning system was 207.2 cGy whereas 204.1 cGy was found with the verification system. The difference in dose for the 3D dose matrix was 5.6 cGy at one standard deviation, cor-

TABLE II. Comparison of computed and measured profiles for all depths (d_{max}, 5, 10, 20, and 30 cm) pooled together after normalization at d_{max} on the central axis to the measured dose rate. Difference at one standard deviation. The number of points for these comparisons ranged from 57 and 1077.

Field size (cm)	2×2	5×5	10×10	25×25	20×20 60° wedge	20×20 60° wedge
Energy (MV)	18	18	18	18	18	6
Inner beam (cGy/MU)	0.006	0.003	0.004	0.008	0.008	0.006
Outer beam (cGy/MU)	0.012	0.002	0.012	0.029	0.002	0.009
Penumbra (cm)	0.07	0.02	0.04	0.15	0.14	0.22

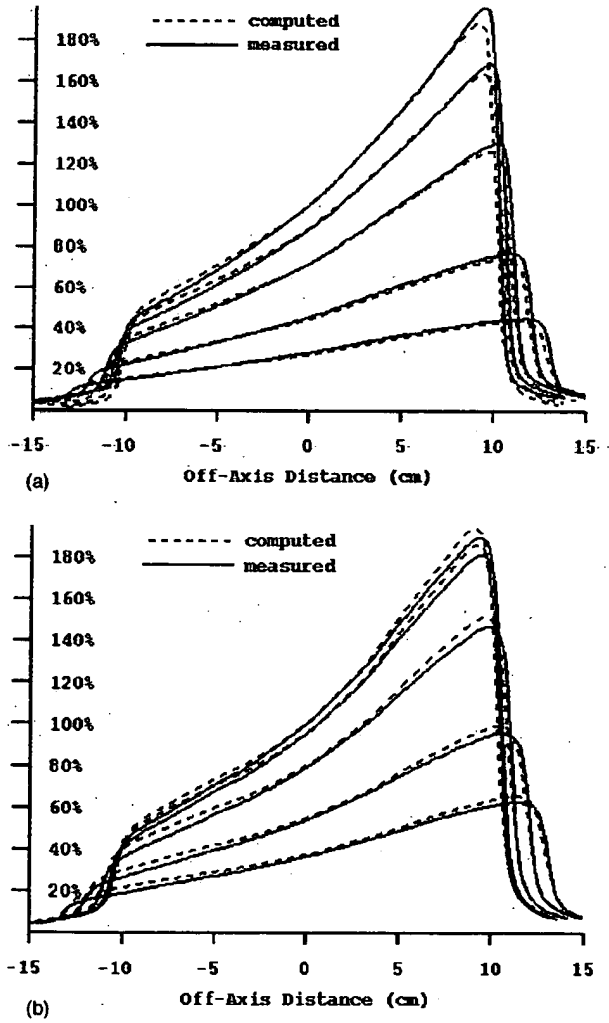

FIG. 3. (a) Measured and computed profiles compared for a 60° wedge, 20×20 cm field size, 6 MV. Depths are 1.7, 5, 10, 20, and 30 cm. Dose normalized to 100% on the central axis at d_{max}. (b) Measured and computed profiles compared for a 60° wedge, 20×20 cm field size, 18 MV. Depths are 3.4, 5, 10, 20, and 30 cm. Dose normalized to 100% on the central axis at d_{max}.

responding to 2.8% of the dose at isocenter. Shown are the isodose lines corresponding to 95%, 80%, and 50% of the isocenter dose of the planning system compared to the dose computed here. Of these data, the 2.8% difference at one standard deviation is probably the most significant, followed by the difference in dose at isocenter of 1%.

E. Example of an IMRT case

Figure 5 shows the transverse slice through isocenter for a case treated with six 6 MV intensity modulated beams. The plan was generated with a commercial inverse planning system (Corvus, Nomos, Swickley, PA) and the beams were delivered with a step and shoot technique.[14,28] Segments with less than 1 MU had to be removed from the plan due to the delivery machine limitation. The total lost MUs were distributed over the remaining segments. It was assumed that this would not alter the delivered plan considerably. The planned dose at the isocenter was 187 cGy, whereas the calculation based on measured intensity patterns here yielded 193 cGy at the isocenter, a 3.2% difference. The doses shown correspond to 95%, 80%, and 50% of the dose at the isocenter.

Shown in Fig. 6 is a dose difference volume histogram for this case. The dose is computed here for each point in the 3D dose matrix imported from the planning system. The difference in dose is sorted into bins of 5 cGy width. The difference at one standard deviation was 7.6 cGy corresponding to

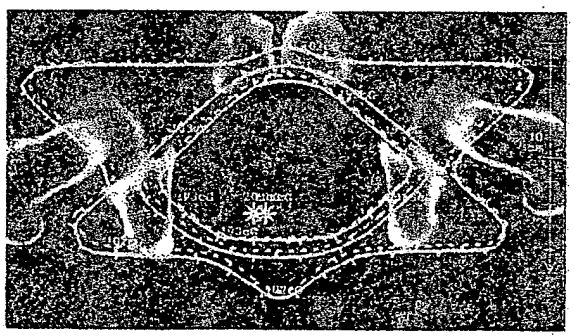

FIG. 4. Example conformal prostate case. 193 cGy corresponds to the 95% isodose line, 163 cGy to 80%, and 102 cGy to 50%. Planning system shown with a dash line, the check shown in with a solid line.

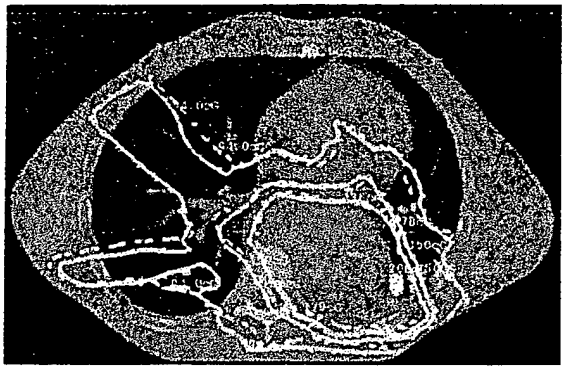

FIG. 5. Comparison of dose from planning system (dash) to that found here for an IMRT case (solid). Doses correspond to 95% (178 cGy), 80% (150 cGy), and 50% (94 cGy) of the stated isocenter dose.

4.1% of the dose at isocenter. The hot spot was computed here to be 226 cGy, whereas the hot spot from the original treatment plan was 223 cGy, a 1.3% difference. These results are felt to be within acceptable criteria for IMRT QA. Large dose differences (in a small volume) do occur in the penumbra regions and are likely due to the approximations used in our delivery verification method, as well as the differences in the dose calculation algorithms which would tend to be emphasized in the lung.

F. Pass–fail criteria

Further work is needed on how to define a pass/fail criteria, or possibly to present the data in some other format. Here the standard deviation of the dose difference, comparing every point from the planning system 3D dose matrix, is probably an important parameter to look at along with the dose at isocenter. The visual comparison of isodose distributions shown in Figs. 4 and 5 is somewhat subjective as the same value isodose curve in low gradient areas can be separated by large distances but might nonetheless represent a relatively small change in actual dose and therefore might not be of consequence. The same problem will exist in comparing isodose curves in phantoms as to defining a pass/fail criteria. Based on isodose curves alone it is difficult to offer an objective pass/fail criteria. The standard deviation of the dose difference for all points and the comparison of the dose at isocenter and the hot spot doses would be more objective.

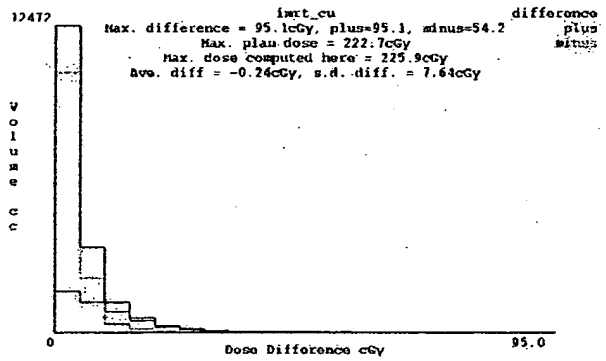

FIG. 6. The difference volume histogram computed for the example case. Each bar is a step in 5 cGy increments. The total difference is shown (upper bar). The two other bars show the histogram for doses that are larger and smaller than the planning system (normally in different colors).

G. Verification considerations

This new approach provides both the absolute dose and the dose distribution in the patient and thus provides a verification loop. Although this procedure does not confirm the correct placement of fields on the patient, it checks if the planned treatment can be accurately delivered.

The time needed to perform this verification includes the time needed for exposing the films, for processing and scanning the films, and to perform the calculations. It takes less than a minute to digitize a film on the film scanner and save the result to a file. The importing of the plan in RTOG format is also very fast. About a half hour is needed to run the delivery verification software including performing dose difference analysis. The use of a portal imaging system that can integrate and measure dose should reduce this effort by eliminating the need to handle, process, and digitize the films. The treatment sequence would simply be performed on the accelerator with the images immediately available for the verification software.

It would seem desirable that the film holding mechanism be attached to the collimator so that the accelerator can be rotated to the intended gantry and collimator angles, rather than place the film on the couch as we have done to demonstrate the feasibility of this method, since the accelerator performance could change with gantry and collimator angle. This same consideration would apply to any other mechanism used to capture images of the treatment fields. But there might be small differences in the collimator scatter factor at such shorter distances and we have not investigated these differences.

The dose calculation algorithms used in our treatment planning system and in the delivery verification system are different. Although both these algorithms have acceptable accuracy in water phantoms, differences in inhomogeneous situations, such as the lung, are likely to be important and should be further investigated. Comparing the dose in a homogeneous phantom also does not address this issue. If the same dose calculation algorithm is used for the initial planning and for the verification dose calculation, the impact of any dose calculation error on the comparison would be expected to be minimal. Hence, using a different dose calculation engine for verification provides some added level of independence, hence redundancy. If both systems have clinically acceptable accuracy, then differences due to algorithmic differences should be small or understandable, for example in interface areas. However, the main purpose remains here to not verify the dose calculation accuracy of the planning system but to verify the delivery.

To make the system suitable for detecting delivery errors, it is important that each step of the process be executed with care. Assuming these steps can be consistently accomplished

and the RMU can be determined from the films to an accuracy of 2%, which is shown to be achievable, the isocenter dose computed here should be able to flag an error in dose greater than 5%. However, since the verification currently only compares the final dose distribution, the cause of an error might not be obvious. For example, if the collimator has a 5 mm error for all the fields, we would expect to see a change in the final dose distribution and be able to determine the error by comparing isodose lines. On the other hand, if only one of six fields were off a small amount, the result might not be as noticeable but would also be less important. If some error occurred that resulted in a change in dose of 5% or more, this change should be detectable. Further investigation of the plan would then be necessary to determine the reason for the discrepancy.

IV. CONCLUSION

A new scheme for verifying the accuracy of beam delivery has been presented. By comparing the dose computed from measured photon fluence distributions with that from the treatment plan, the method provides a means to verify the accuracy of the treatment plan delivery on the same patient anatomy. Both the absolute dose and the dose distribution can be compared. Validations of the new scheme showed that the system is capable of achieving accuracy better than 5% with film. The data transfer and analysis tools increase the usefulness and efficiency. Since only one dry-run is needed for the verification, the system can significantly reduce the QA time for IMRT delivery. When combined with a suitable portal imaging system, the time needed for delivery verification should be further reduced.

[a]Electronic mail: wendeldrenner@comcast.net

[1]K.L. Pasma, M.L.P. Dirkx, M. Kroonwijk, and A.G. Visser, "Dosimetric verification of intensity modulated beams produced with dynamic multileaf collimation using an electronic portal imaging device," Med. Phys. 26, 2373–2378 (1999).

[2]R. Boellaard, M. van Herk, and B.J. Mijnheer, "New method to obtain the midplane dose using portal in vivo dosimetry," Int. J. Radiat. Oncol., Biol., Phys. 41, 465–474 (1998).

[3]M. Partridge, M. Ebert, and B-M. Hesse, "IMRT verification by three-dimensional dose reconstruction from portal beam measurements," Med. Phys. 29, 1847–1858 (2002).

[4]G.J. Kutcher *et al.*, "Comprehensive QA for radiation oncology," Med. Phys. 21, 581–618 (1994).

[5]B. Fraass, K. Doppke, M. Hunt, G. Kutcher, G. Starkschall, R. Stern, and J. Van Dyke, "American Association of Physicist in Medicine Radiation Therapy Committee Task Group 53: Quality assurance for clinical radiotherapy treatment planning," Med. Phys. 25, 1773–1829 (1998).

[6]V. Hansen, P. Evans, G. Budgell, J. Mott, P. Williams, M. Brugmans, F. Wittkamper, B. Mijnheer, and K. Brown, "Quality assurance of the dose delivered by small radiation segments," Phys. Med. Biol. 43, 2665–2675 (1998).

[7]G. Budgell, C. Martens, and F. Claus, "Improved delivery efficiency for step and shoot intensity modulated radiotherapy using a fast-tuning magnetron," Phys. Med. Biol. 46, N253–N261 (2001).

[8]G. Ezzell and S. Chungbin, "The overshoot phenomenon in step-and-shoot IMRT delivery," J. Appl. Clin. Med. Phys. 2, 138–148 (2001).

[9]T. LoSasso, C.S. Chiu, and C.C. Ling, "Physical and dosimetric aspects of a multileaf collimation system used in the dynamic mode for implementing intensity modulated radiotherapy," Med. Phys. 25, 1919–1927 (1998).

[10]L. Ma, P. Geis, and A. Boyer, "Quality assurance for dynamic multileaf collimator modulated fields using fast beam imaging system," Med. Phys. 24, 1213–1220 (1997).

[11]D.A. Low, R.L. Gerber, S. Mutic, and J.A. Purdy, "Phantoms for IMRT dose distribution measurement and treatment verification," Int. J. Radiat. Oncol., Biol., Phys. 40, 1231–1235 (1998).

[12]B. Paliwal and W. Tome, "A spiral phantom for IMRT and tomotherapy treatment delivery verification," Med. Phys. 27, 2503–2507 (2000).

[13]J.S. Li, A.L. Boyer, and C.M. Ma, "Verification of IMRT dose distributions using a water beam imaging system," Med. Phys. 28, 2466–2474 (2001).

[14]C. Yu *et al.*, "A method for implementing dynamic photon beam intensity modulation using independent jaws and a multileaf collimator," Phys. Med. Biol. 40, 769–787 (1995).

[15]J. Esthappan, S. Mutic, W. Harms, and J. Dempsey, "Dosimetry of therapeutic photon beams using an extended dose range film," Med. Phys. 29, 2438–2445 (2002).

[16]N.L. Childress, L. Dong, and I.I. Rosen, "Rapid radiographic calibration for IMRT verification using automated MLC fields," Med. Phys. 29, 2384–2390 (2002).

[17]I.J. Yeo and C. Wang, "A filtration method for improving film dosimetry in photon radiation therapy," Med. Phys. 24, 1943–1953 (1997).

[18]T.R. Mackie, A.F. Bielajew, D.W.O. Rogers, and J.J. Battista, "Generation of photon energy deposition kernels using the EGS Monte Carlo code," Phys. Med. Biol. 33, 1–20 (1988).

[19]A. Ahnesjo, "Collapsed cone convolution of radiant energy for photon dose calculation in heterogeneous media," Med. Phys. 16, 577–592 (1989).

[20]H.H. Liu, T.R. Mackie, and E.C. McCullough, "Correcting kernel tilting and hardening in convolution/superposition dose calculation for clinical divergent and polychromatic photon beams," Med. Phys. 24, 1729–1741 (1997).

[21]A. Ahnesjo, M. Saxner, and A. Trepp, "A pencil beam model for photon dose calculation," Med. Phys. 19, 263–273 (1992).

[22]M.D. Altschuler, P. Bloch, E.L. Buhle, and S. Ayyalasomayajula, "3-D dose calculations for electron and photon beams," Phys. Med. Biol. 37, 391–411 (1992).

[23]J. Van Dyk, R.B. Barnett, J.E. Cygler, and P.C. Shragge, "Commissioning and quality assurance of treatment planning computers," Int. J. Radiat. Oncol., Biol., Phys. 26, 261–273 (1993).

[24]Task Group #23, *Radiation Treatment Planning Dosimetry Verification*, AAPM Report 55 (American Association of Physics in Medicine, College Park, MD, 1995).

[25]H. Liu, T. Mackie, and E. McCullough, "Calculating output factors for photon beam radiotherapy using a convolution/superposition method based on a dual source photon beam model," Med. Phys. 24, 1975–1985 (1997).

[26]I.J. Chetty and P.M. Charland, "Investigation of Kodak Extended Dose Range (EDR) Film for megavoltage photon beam dosimetry," Phys. Med. Biol. 47, 3629–3641 (2002).

[27]W.D. Renner, T.P. O'Connor, and N.M. Bermudez, "An algorithm for design of beam compensators," Int. J. Radiat. Oncol., Biol., Phys. 17, 227–234 (1989).

[28]C.S. Chui, S. Spirou, and T. LoSasso, "Testing of dynamic multileaf collimation," Med. Phys. 23, 635–641 (1996).